Hindawi Publishing Corporation
International Journal of Photoenergy
Volume 2014, Article ID 141368, 8 pages
http://dx.doi.org/10.1155/2014/141368

Research Article

Effect of Ce Doping on RGO-TiO_2 Nanocomposite for High Photoelectrocatalytic Behavior

Md. Rakibul Hasan, Chin Wei Lai, Sharifah Bee Abd Hamid, and Wan Jeffrey Basirun

Nanotechnology and Catalysis Research Centre (NANOCAT) and Institute of Postgraduate Studies, University of Malaya, Level 3, Block A, 50603 Kuala Lumpur, Malaysia

Correspondence should be addressed to Chin Wei Lai; cwlai@um.edu.my and Sharifah Bee Abd Hamid; sharifahbee@um.edu.my

Received 14 December 2013; Revised 13 January 2014; Accepted 13 January 2014; Published 15 April 2014

Academic Editor: Jiaguo Yu

Ce doped RGO-TiO_2 composite films on ITO substrates were prepared by sol-gel process using tetrabutyl titanate and reduced graphene oxide (RGO) as the starting materials. The sample was designed for the photoelectrocatalytic applications. The obtained samples were characterized by X-ray diffraction, UV-vis absorption spectroscopy, scanning electron microscopy, and Fourier transformed infrared spectroscopy. The results showed that doping of Ce on RGO-TiO_2 composite film inhibited the TiO_2 anatase-rutile phase transformation. In this case, Ce atoms could serve as dispersion oxide and suppress the recombination of photoinduced electron-hole pairs. Besides, the change in absorbance from UV to visible region was observed in Ce doped RGO-TiO_2 nanocomposite films. The Ce doped RGO-TiO_2 composite film showed higher photoelectrochemical performance than that of RGO-TiO_2 composite and pure TiO_2 under solar simulator irradiation. The main reason might be attributed to the optimum content of Ce that could act as electrons acceptor to hinder the recombination loss and facilitate the better transportation for photoinduced charge carriers.

1. Introduction

Today, high performance photoactive electrode is considered to be one of the probable solutions for utilization of solar energy. Efficient photoelectrocatalysis (PEC) process is greatly dependent on such an electrode surface which shows high photon absorption, less photocorrosion, mesoporous surface structure, and highly dispersed uniform active sites [1]. Various metal oxides, carbon nanomaterials, and so forth have been extensively investigated for photocatalytic applications such as H_2 production from water splitting, pollutants degradation, dye sensitized solar cells, and CO_2 photoreduction [2, 3]. But the overall photocatalytic performance under visible irradiation is still not satisfactory. Photocatalytic redox reaction under visible light irradiation can be enhanced by applying little bias potential and this electroassisted photocatalysis is called the photoelectrocatalysis (PEC) process.

After the invention of graphene in 2004, this two-dimensional sp2 bonded honeycomb-like carbon nanomaterial brought a massive change in electronics and solar and energy management devices. Reduced graphene oxide (RGO) support on photoelectrodes showed high electron mobility and high thermal resistivity and stability [4]. On the other hand, TiO_2, which is already commercially established as a photocatalyst material, shows better performance as catalyst support due to stability in chemical solution and its tunable textural properties. Although TiO_2 possesses excellent optoelectronic properties under UV irradiation, it shows poor absorption under visible light due to its wide band gap value of 3.2 eV. However, recent research showed that RGO-TiO_2 composite material can show higher photocatalytic activity under visible light [5–7]. This is due to broad expanse of the electronic state of RGO-TiO_2 coupling. Moreover, this coupling possesses high adsorption capacity, extended light absorption range, and enhanced charge separation and transportation properties [8].

Nevertheless, the difficulties of catalyst recovery, low visible light absorption, and fast recombination of electron-hole pairs are still the main pitfalls of using powder photocatalyst in aqueous media [9]. These drawbacks are crucial indeed

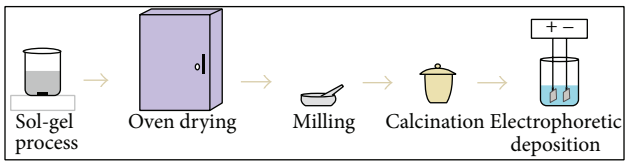

Figure 1: Schematic diagram of the experimental procedure.

for viable large scale applications like H_2 production from water and CO_2 conversion into useful fuels. However, the catalyst recovery and recycling difficulties can be avoided to a great extent using thin film photocatalysts. And the process when assisted with electrochemical bias can help to improve the overall efficiency of the photocatalytic process [10, 11]. Other than RGO-TiO_2 composite film, some other transition metal oxides such as ZnO, ZrO_2, NbO_5, and V_2O_5 also showed promising outcome in photocatalytic process [12, 13]. But in terms of stability and longtime functionality, both of the materials RGO and TiO_2 got benchmark performance in different photocatalytic activities like water splitting and dye degradation [14, 15]. It is noted that, even though RGO-TiO_2 can enhance their synergistic effects over a photocatalysis process, the electron-hole separation upon visible light irradiation is energetically unstable and recombination rates are very fast on the order of nanoseconds [16]. Experimental results showed that controlled charge separation in photoelectrocatalysis process rectifies electron transfer on the photocatalyst film and it also increases the electron availability on the conducting substrates.

The photocatalytic activity of RGO-TiO_2 composite can be more enhanced either by promoting the light absorption or by suppressing the electron-hole recombination rate through the incorporation of other species to the binary composites [17]. Some rare earth oxides show polymorphism, good thermal stability and good light absorption, and so forth due to their multielectron atoms including f orbital electrons. Previous experiments proved that, Ce ion, a rare earth metal which has the ability to enhance the photocatalytic activity of TiO_2 [18, 19]. This is due to the presence of different electronic structures (Ce^{3+}/Ce^{4+}) of cerium ion which show different electronic and optical properties of the catalyst. Thus, RGO-TiO_2 composite photocatalyst doped with Ce can act as exciton trap and might retard the fast electron/hole recombination. In essence, it can help to increase available photoelectrons on the surface. In the present study, we prepared Ce doped RGO-TiO_2 composite powder via sol-gel method and thin film photocatalyst was prepared via electrophoretic deposition method (Figure 1). Solar simulator was used to stimulate the thin film photocatalyst and studied in the PEC process. The photoelectrocatalytic conversion performance of the films as-prepared was examined, and the interesting results were obtained.

2. Experimental Methods

2.1. Catalyst Powder Preparation. Tetra-n-butyl orthotitanate (TBOT) was procured from Sigma-Aldrich and all other chemicals used in this work were of analytical grade. The indium tin oxide (ITO) coated conducting glass plates (0.7 mm thickness) were procured from Osaka, Japan. Graphene oxide was prepared via modified Hummer's method [20, 21]. Hydrazine treatment was done to obtain reduced graphene oxide (RGO) [22]. For the preparation of TiO_2, 4 mL TBOT was added with 20 mL of absolute ethanol and kept under stirring. This solution was added dropwise to a mixture of 2 mL of DI water and 1 wt% of cerium nitrate hexahydrate. Acetic acid was added to the mixture to keep the pH <3. This was followed by the addition of 1 wt% RGO, 2 mL of deionized water, and 5 mL ethanol and kept under sonication for 1 hour. This solution was added gradually with the previous solution. The total mixture was stirred for 30 minutes and kept for 24 hours for gel formation. The gel was dried at 70°C overnight. The dry porous gel was milled using mortar and pestle. The dried catalyst powder was calcined at 550°C for 4 h. The same procedure was followed to prepare RGO-TiO_2 composite and pure TiO_2 powder.

2.2. Thin Film Preparation. ITO coated glass substrate was cleaned with acetone, dehydrated alcohol, and ultrapure water, respectively. The powder photocatalyst was deposited on the ITO coated substrate via electrophoretic deposition method [23]. A DC power supply was used for the necessary current-voltage application. The substrate was cut into a 1 cm × 1 cm working area and used as both anode and cathode. The electrolyte composition was prepared at 1 mg/mL powder catalyst by sonication before the deposition process. The applied voltage was 60 V and deposition time was 1 min.

2.3. Characterizations of Catalysts. XRD spectra were recorded with a powder X-ray diffractometer (type Bruker D8 Advance equipped with EVA diffract software, Germany) over the range $20^\circ \leq 2\theta \leq 80^\circ$, operating at 40 kV and 40 mA, using Cu Kα radiation (k = 1.5418 A). A scanning electron microscope (SEM, Quanta FEI 200) was used to probe the coating materials on the surface of ITO coated glass substrates. A UV-vis spectrophotometer from PerkinElmer, Lambda 35 series, equipped with a 10 mm path length quartz cell was used for UV spectroscopic measurement. Fourier transformed infrared (FTIR) spectroscopy was recorded using a Bruker IFS 66V/S using a KBr technique.

All photoelectrochemical experiments were carried out with an Autolab PGSTAT302N potentiostat/galvanostat (EcoChemie, The Netherlands) with a three-electrode quartz cell. Ce-RGO-TiO_2/ITO, RGO-TiO_2/ITO, and TiO_2/ITO modified electrodes were used as the working electrode. A saturated calomel electrode (SCE) was used as the reference and a platinum wire was used as the counter electrode. A 0.1 M Na_2SO_4 solution was used as a supporting electrolyte. An active area of 1.0 cm^2 working electrodes for each sample was used in the photocurrent experiments. A 150 W solar simulator was used as a light source to study the photoelectrochemical response (Figure 2). The photocurrent was measured for the Ce-RGO-TiO_2 and the RGO-TiO_2 modified composite electrode at an applied potential of 0.02 V (SCE).

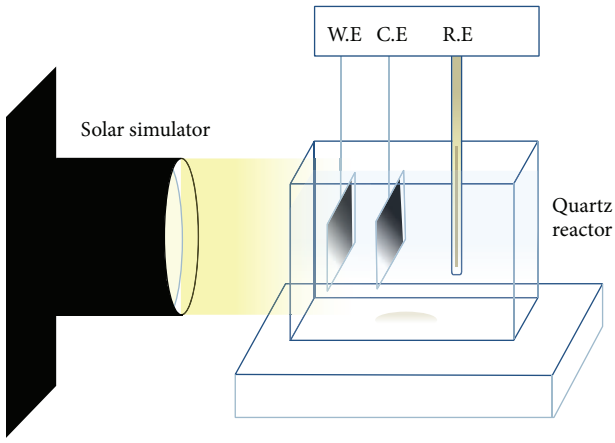

Figure 2: Quartz made photoelectrocatalytic (PEC) reactor with solar simulator.

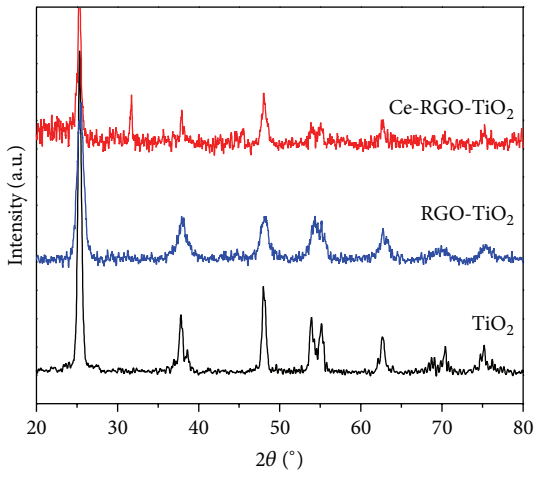

Figure 3: XRD pattern of pure TiO_2, RGO-TiO_2, and Ce-RGO-TiO_2.

3. Results and Discussion

The samples were collected by scraping off the pure TiO_2, RGO-TiO_2, and Ce doped RGO-TiO_2 from the ITO coated electrodes for XRD measurements to confirm that the samples are well crystallized. According to JCPDS data (reference code 832243), the peaks at 25.4° (1 0 1), 38.5° (1 1 2), and 48.6° (2 0 0) are the characteristic diffraction pattern of the anatase phase. The diffraction patterns are shown in Figure 3. No phase change from anatase to rutile was found in the samples although the calcination temperature was 550°C. In fact, the phase transformation can occur from anatase to rutile at 500–700°C [24]. Thus, the presence of Ce atoms can block the anatase-rutile phase transformation for TiO_2 [25]. The average crystallite size was calculated using Scherrer's formula (1) with respect to the anatase peaks. Consider

$$D = \frac{0.89\lambda}{\beta \cos\theta}, \quad (1)$$

where D = crystallite size, λ = wavelength of X-ray, β = full width at half maximum of the peak (in radians), and θ = angle of diffraction (in degrees) [26].

The crystallite size for the RGO-TiO_2 was between 40 and 62 nm which is similar to the pure TiO_2 nanoparticles. So, it can be concluded that RGO has no effect on the crystal structure of TiO_2 [27]. But, for Ce-RGO-TiO_2, the crystallite size was between 35 and 45 nm with respect to the Ti-anatase peaks which is lower than the RGO-TiO_2 or pure TiO_2. Thus, Ce atoms can suppress the growth of TiO_2 crystallite size. Moreover, due to the large difference in atomic radius between Ce and Ti (204 and 160 pm, resp.), the cations cannot be incorporated with each other. It is assumed that Ce atoms are dispersed on the surface of TiO_2. The XRD pattern for 1% Ce doped RGO-TiO_2 shows a characteristic peak for Ce at 33.09°. According to JCPDS reference code 340394, the peak is attributed to CeO_2 (2 0 0) plane. other peaks are not obvious due to high dispersion of CeO_2 on RGO-TiO_2 surface.

Figure 4 shows the SEM images of Ce-RGO-TiO_2 and RGO-TiO_2. It could be observed that while Ce-RGO-TiO_2 composite approximately exists in the form of spherical particles, RGO-TiO_2 exists mostly as granular structure. RGO could help the TiO_2 nanoparticles to disperse more smooth and uniform whereas Ce particles can improve the stability of the active phase. And, hence, the film surface was even and the film strength was observed to be higher than pure TiO_2. The thickness of the films was found to be roughly 2 μm. 1% RGO loading showed more homogeneous dispersion and electrochemical stability than higher percentage of RGO loading. Cerium atom dispersion with the RGO-TiO_2 structure has made the material more porous and hence the available active sites for redox reactions have increased. The average size was about ~40 nm, according to the value determined by XRD.

The morphology of Ce-RGO-TiO_2 was also observed with TEM. Figure 5 shows the porous structure with crystallite size below 50 nm which is well suited with XRD and SEM results. Agglomeration over the grain boundaries was observed in TiO_2 nanoparticles due to Ce doping.

The optical absorption spectra of the samples are shown in Figure 6. The RGO-TiO_2 and Ce doped RGO-TiO_2 showed higher photoabsorption in the visible region (>400 nm) compared to the pure TiO_2. Pure titania anatase showed an absorption edge at ~387 nm, while RGO incorporated TiO_2 also showed absorption at the same wavelength but with higher intensity. More photon absorption was observed for Ce-RGO-TiO_2 as well. Band gap values were determined by the following equation:

$$E_{bg} = \frac{1240}{\lambda}\ (\text{eV}), \quad (2)$$

where E_{bg} = band gap energy of the photocatalyst material and λ = maximum wavelength in nm.

A reduced band gap value was expected but no significant change in band gap energy was observed. This could be due to the aggregation of RGO material and the electron trap effect of ceria nanoparticles. The band gap energy was not much reduced and maximum absorption was still in the UV region for the modified TiO_2 samples. Nevertheless, more

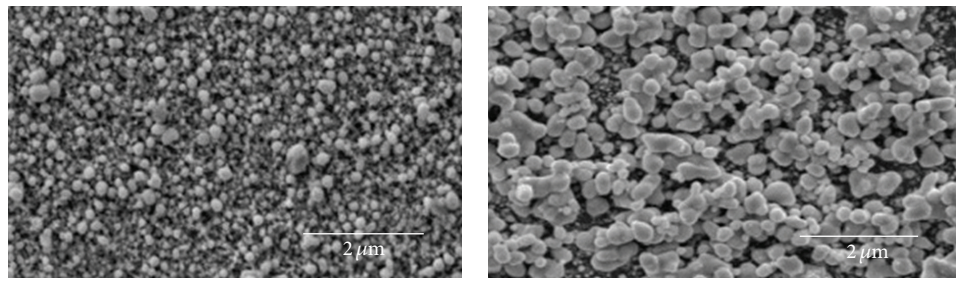

(a) (b)

Figure 4: SEM image of (a) RGO-TiO_2 and (b) Ce-RGO-TiO_2 coated ITO substrate.

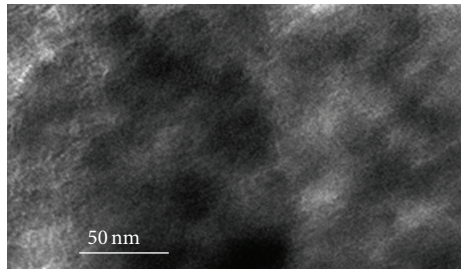

Figure 5: TEM image of Ce-RGO-TiO_2.

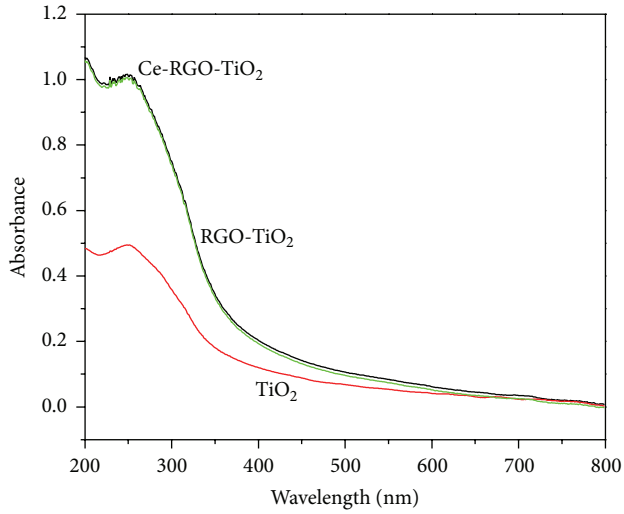

Figure 6: Effect of Ce loading on UV absorbance in RGO-TiO_2 photocatalysts.

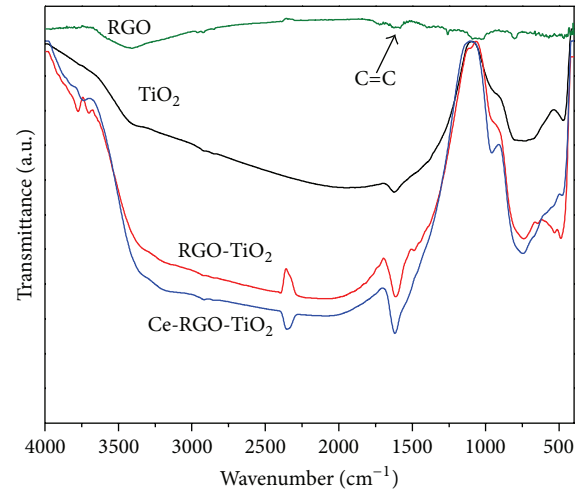

Figure 7: FTIR spectra of Ce doped RGO-TiO_2 composites.

photoelectrons can be produced using UV light source and it will ease the photocatalytic reduction process due to available electrons on the catalyst surface. It is clear that both RGO and Ce particles showed an enhanced photon absorption property in this respect.

The FTIR spectra of the samples were presented in Figure 7. It can be observed that, in RGO, most of the peaks for oxygen functional groups were eliminated whereas C=C skeletal vibration of graphene sheet is obvious at 1580 cm^{-1} [28]. It confirms that graphene oxide was reduced well and the surface became hydrophobic. In TiO_2, the broad peaks at 580 and 1050 cm^{-1} can be attributed to Ti–O–Ti and Ti–O stretching vibrations [29]. A band that slightly shifted from 1500 cm^{-1} in both RGO-TiO_2 and Ce-RGO-TiO_2 was also observed. It is attributed to the graphene sheet skeletal vibrations. The broad bands below 1000 to 600 cm^{-1} in TiO_2 composites can be assigned to Ti–O stretching vibrations [30]. The weak peak below 500 cm^{-1} in Ce-RGO-TiO_2 sample denotes Ce-O vibrational stretch [31].

The cyclic voltammetry for RGO-TiO_2/ITO and Ce-RGO-TiO_2/ITO modified electrodes are shown in Figure 8. The scan rate was fixed at 50 mV/s in the range of −1 V to +1 V. It is observed that both positive extraction peak and negative injection peak for RGO-TiO_2 and Ce-RGO-TiO_2 are obvious with little peak current. In the dark, both samples showed almost same characteristic peaks with a very small peak current (Table 1). But under visible light irradiation, both extraction and injection peaks are enhanced obviously. The Ce-RGO-TiO_2 showed the highest peak current while illumination, although Ce doping in RGO-TiO_2 did not enhance current efficiency in dark.

It can be concluded that Ce atoms can absorb photons and transfer to the electrons that gain more energy to produce photocurrent. 1% Ce doping showed an optimal

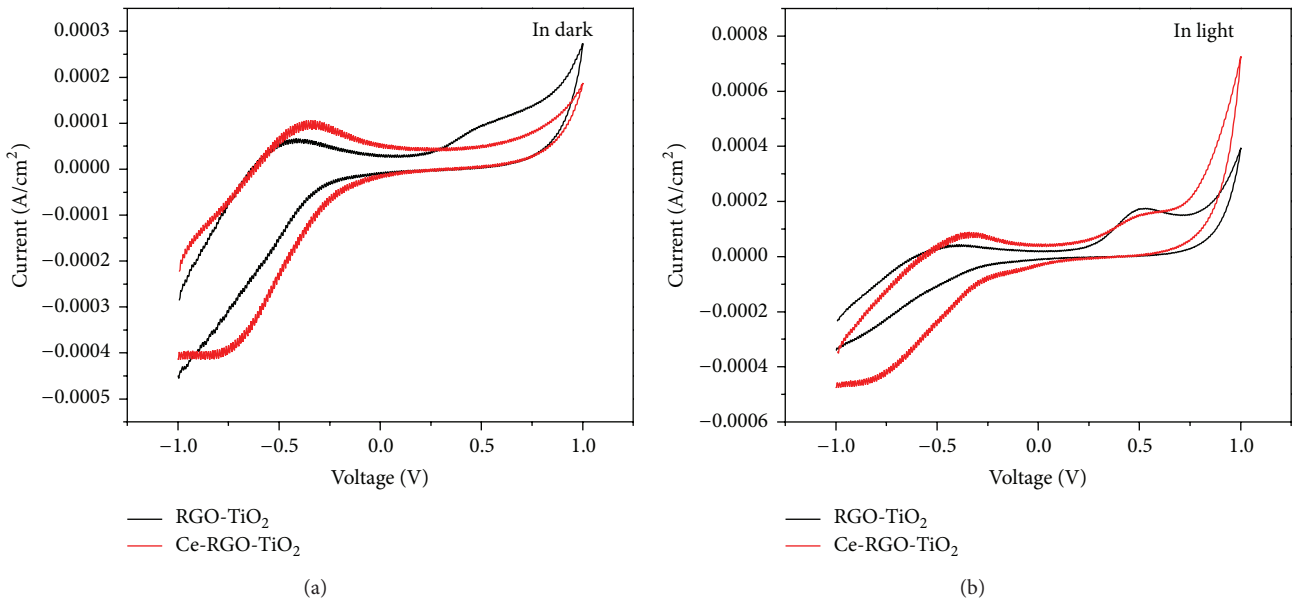

Figure 8: Cyclic voltammogram of catalytic activity with RGO-TiO_2/ITO and Ce-RGO-TiO_2/ITO modified electrodes in both dark and visible light irradiation.

Table 1: Peak current table for RGO-TiO_2 and Ce doped RGO-TiO_2 thin films (values in mA/cm^2).

Peak current	RGO-TiO_2 thin film		Ce doped RGO-TiO_2 thin film	
	Dark	Light	Dark	Light
+ve extraction peak current	0.3	0.3	0.2	0.7
−ve injection peak current	0.4	0.4	0.4	0.6

photocurrent value of 0.74 mA/cm^2. The RGO-TiO_2 sample showed another minor peak at 0.58 V both in dark and under light illumination. But that peak vanished in Ce-RGO-TiO_2 sample. The reason behind this could be due to the defect formation in octahedral TiO_2 structure from the doping with Ce. The regular TiO_2 octahedron structure became distorted and highly amorphous. This structure provided more open spaces in the crystal lattice and facilitated electron trapping. That could hide the minor peak current formation.

The photoelectrochemical performance is largely dependent on charge transfer and recombination properties of a photocatalyst material. In this case, electrochemical impedance spectrum (EIS) is very useful tool to investigate the charge carriers transfer and recombination processes at semiconductor/electrolyte interfaces. The samples were investigated for EIS responses and the components of complex impedance Z were plotted as Z'' (imaginary part) versus Z' (real part) in Nyquist plot (Figure 9).

The values were measured at open circuit potential for both dark and light irradiation periods. It can be observed that the samples formed pseudoarcs in the Nyquist plot for both dark and light irradiation periods. Under light irradiation, the photogenerated electrons moved from the electrode surface to the outer circuit. This phenomenon helped to reduce the interface resistance. Thus, the diameter of the loops was also reduced under light irradiation. The diameter of the loops was reduced for Ce doped RGO-TiO_2 samples as well. In fact, graphene can also show synergistic effect with doped metal atoms (here Ce) in terms of reducing charge transfer resistance [32]. In this case, the hybridization of Ce on RGO-TiO_2 composites leads to high-speed charge transport properties. This is due to the excellent Ce light absorption and ultrahigh electron mobility in graphene structures. The diameter actually reflects the rate of electron transfer which also indicates the photocatalytic reaction rate [1]. The equivalent circuit with the corresponding Nyquist plot is shown in Figure 10.

It can be simulated with Warburg semi-infinite diffusion model where a double layer capacitance and a charge transfer impedance are added with Warburg diffusion impedance. Here, polarization that occurred was influenced by the kinetic and diffusion processes and it can be interpreted by the Warburg model simulation. Here, R_s denotes the solution resistance. It showed the resistance value literally where the semicircle intercepts with the real axis at high frequency region. In this model, the passivation reaction was proposed and the resistance between the space charge layer and open Helmholtz layer was considered dependent on the double layer capacitance (C_{dl}) and charge transfer resistance (R_{ct}).

A simple mechanism of photoelectron excitation was illustrated in Figure 11. When light was illuminated with sufficient photon energy, the electron transfer happens from O (2p) valence band to Ti (3d) conduction band. The Ce

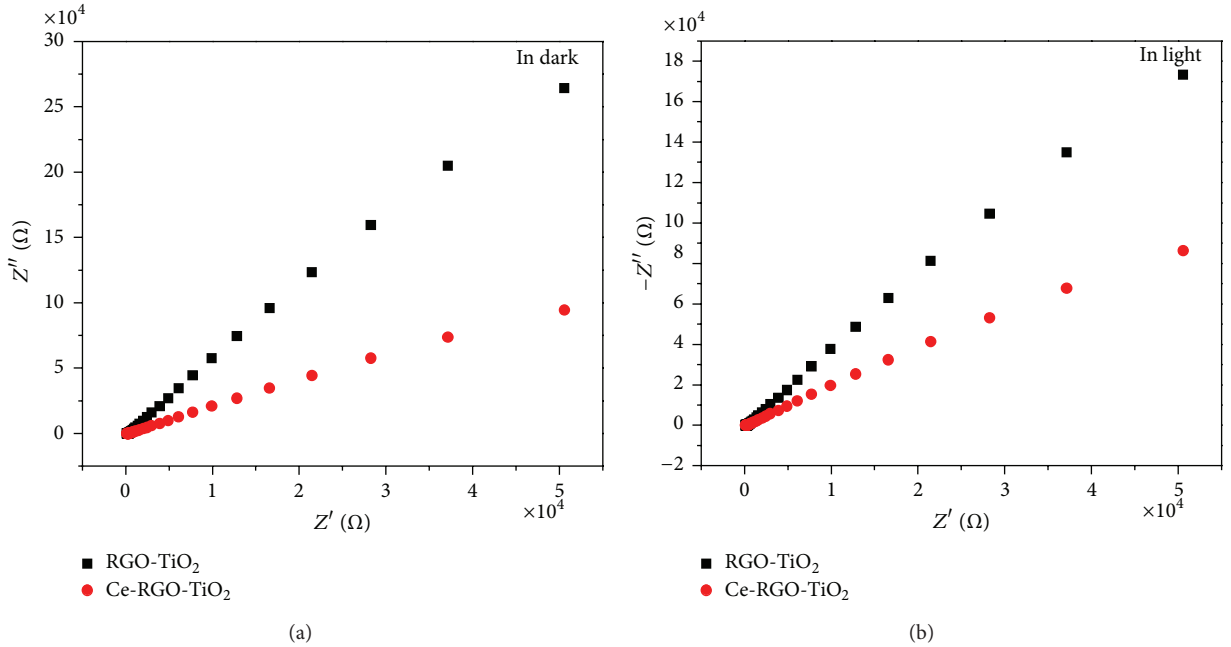

Figure 9: The EIS responses (Nyquist plots) of the RGO-TiO_2 and Ce doped RGO-TiO_2 film electrodes with and without light irradiation at open circuit potential (in dark) and at open circuit potential under visible light irradiation.

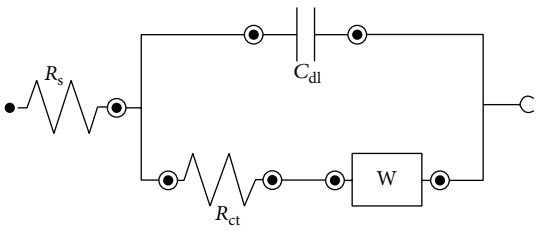

Figure 10: Warburg impedance simulation cell (equivalent circuit with mixed kinetic and charge transfer control).

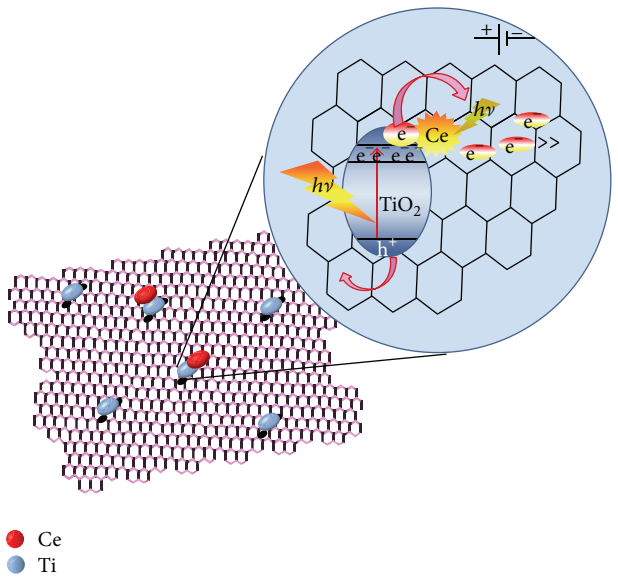

Figure 11: A schematic diagram of Ce doped RGO-TiO_2 composite and a rough presentation of photoelectron release mechanism.

atoms also absorb photon energy and transfer it to the photoelectrons. This incident drives the electrons intensely and it helps to reduce the recombination of electron-hole pairs.

The Ce atoms also act as a charge carrier trap. And finally, with the help of a little outer circuit bias, the electrons move steadily towards counter electrode. RGO π-electron conjugation structure favors the electron movement in this regard. Thus, electrons become available on counter electrode for redox species to be reduced, leaving the holes for the other species to be oxidized. Thus, the photocatalytic reaction proceeds and the photocurrent generated from the reaction becomes the driving force for the reaction. The whole process is still unclear to the researchers and we are lacking great deal of information about different behaviors of catalyst material towards different redox species. However, a combination of both theoretical and experimental results will help to understand in detail the PEC process.

When a semiconductor is dipped into an electrolyte containing redox species, the chemical potentials of electrons on both semiconductor and redox species will try to be in equilibrium. The charge transfer across the semiconductor surface will generate a space charge layer and band bending will occur. This is to minimize the effect of space charge layer in the semiconductor. Eventually, a potential barrier

is established so that further electron transfer could not occur. Under illumination, the space charge layer is weakened due to electron-hole separation [1]. The photons push the electrons inside the bulk of the semiconductor and thus the holes come out on the surface. Ultimately, the band bending decreases and it facilitates the movement of electrons towards outer circuit that is to the counter electrode. Thus, the photocurrent develops when the holes start to react with the redox species present in the electrolyte. The electron-hole separation can be enhanced by applying a small bias voltage to form overpotential on the electrode. This overpotential changes the width of the space charge layer and hinders the recombination of electron-hole pairs. Thus, more and more active species are oxidized on the semiconductor surface and photoelectrocatalytic process continues.

4. Conclusions

Ce doped RGO-TiO_2 composite thin films were prepared by sol-gel and electrophoretic deposition method. The sample showed enhanced photoelectrocatalytic activity compared to pure TiO_2 and RGO-TiO_2 composite films. The experiment was conducted under visible light irradiation. ITO immobilized Ce doped RGO-TiO_2 composite film can be an effective photocatalyst material with the assistance of electrochemical activity. Cerium atom absorbs photon at a higher degree and active photogenerated holes and electrons can be produced by applying an external bias. The excitons can be rectified towards efficient oxidation-reduction reaction. ITO glass substrate can provide a better route for the redox reactions to take place. Above all, the sample showed better stability even after 5-hour irradiation period. Further study is needed to understand the enhanced material efficiency.

Conflict of Interests

The authors declare that there is no conflict of interests regarding the publication of this paper.

Acknowledgment

The authors would like to thank University of Malaya for sponsoring this work under National Nanotechnology Directorate (NND-53-02031090), High Impact Research (HIR-F-000032) and IPPP grant (PG043-2012B) for their cordial support to complete this work.

References

[1] X. Meng, J. Yao, F. Liu et al., "Preparation of SnO_2@C-doping TiO_2 nanotube arrays and its electrochemical and photoelectrochemical properties," *Journal of Alloys and Compounds*, vol. 552, pp. 392–397, 2013.

[2] S. Morales-Torres, L. M. Pastrana-Martínez, J. L. Figueiredo, J. L. Faria, and A. M. T. Silva, "Design of graphene-based TiO_2 photocatalysts—a review," *Environmental Science and Pollution Research*, no. 19, pp. 3676–3687, 2012.

[3] Q. Xiang, J. Yu, and M. Jaroniec, "Graphene-based semiconductor photocatalysts," *Chemical Society Reviews*, vol. 41, no. 2, pp. 782–796, 2012.

[4] Q. Xiang and J. Yu, "Graphene-based photocatalysts for hydrogen generation," *The Journal of Physical Chemistry Letters*, vol. 4, no. 5, pp. 753–759, 2013.

[5] Z. Huimin, S. Fang, F. Xinfei, Y. Hongtao, W. Dan, and Q. Xie, "Graphene-TiO_2 Composite Photocatalyst with Enhanced Photocatalytic Performance," *Chinese Journal of Catalysis*, no. 33, pp. 777–782, 2012.

[6] W. Geng, H. Liu, and X. Yao, "Enhanced photocatalytic properties of titania-graphene nanocomposites: a density functional theory study," *Physical Chemistry Chemical Physics*, vol. 15, no. 16, pp. 6025–6033, 2013.

[7] Y. Zhang, N. Zhang, Z. R. Tang, and Y. J. Xu, "Improving the photocatalytic performance of graphene-TiO_2 nanocomposites via a combined strategy of decreasing defects of graphene and increasing interfacial contact," *Physical Chemistry Chemical Physics*, vol. 14, no. 25, pp. 9167–9175, 2012.

[8] L. Zhang, H. H. Mohamed, R. Dillert, and D. Bahnemann, "Kinetics and mechanisms of charge transfer processes in photocatalytic systems: a review," *Journal of Photochemistry and Photobiology C: Photochemistry Reviews*, vol. 13, no. 4, pp. 263–276, 2012.

[9] A. Panniello, M. L. Curri, D. Diso et al., "Nanocrystalline TiO_2 based films onto fibers for photocatalytic degradation of organic dye in aqueous solution," *Applied Catalysis B: Environmental*, vol. 121-122, pp. 190–197, 2012.

[10] M. Zhang, S. Yuan, Z. Wang, Y. Zhao, and L. Shi, "Photoelectrocatalytic properties of Cu2+-doped TiO_2 film under visible light," *Applied Catalysis B: Environmental*, vol. 134-135, pp. 185–192, 2013.

[11] G. Li, Y. Zhang, H. Sun et al., "Photocatalytic and photoelectrocatalytic degradation of small biological compounds: a case study of uridine," *Catalysis Today*, vol. 201, pp. 167–174, 2013.

[12] T. Inoue, A. Fujishima, S. Konishi, and K. Honda, "Photoelectrocatalytic reduction of carbon dioxide in aqueous suspensions of semiconductor powers," *Nature*, vol. 277, no. 5698, pp. 637–638, 1979.

[13] H. Inoue, H. Moriwaki, K. Maeda, and H. Yoneyama, "Photoreduction of carbon dioxide using chalcogenide semiconductor microcrystals," *Journal of Photochemistry and Photobiology A*, vol. 86, no. 1–3, pp. 191–196, 1995.

[14] Q. Xiang, J. Yu, and M. Jaroniec, "Enhanced photocatalytic H_2-production activity of graphene-modified titania nanosheets," *Nanoscale*, vol. 3, no. 9, pp. 3670–3678, 2011.

[15] C. Zhai, M. Zhu, F. Ren, Z. Yao, Y. Du, and P. Yang, "Enhanced photoelectrocatalytic performance of titanium dioxide/carbon cloth based photoelectrodes by graphene modification under visible-light irradiation," *Journal of Hazardous Materials*, vol. 263, part 2, pp. 291–298, 2013.

[16] X. Y. Zhang, H. P. Li, X. L. Cui, and Y. Lin, "Graphene/TiO_2 nanocomposites: synthesis, characterization and application in hydrogen evolution from water photocatalytic splitting," *Journal of Materials Chemistry*, vol. 20, no. 14, pp. 2801–2806, 2010.

[17] M. R. Hoffmann, S. T. Martin, W. Choi, and D. W. Bahnemann, "Environmental applications of semiconductor photocatalysis," *Chemical Reviews*, vol. 95, no. 1, pp. 69–96, 1995.

[18] T. D. Nguyen, C. T. Dinh, and T. O. Do, "A general procedure to synthesize highly crystalline metal oxide and mixed oxide

nanocrystals in aqueous medium and photocatalytic activity of metal/oxide nanohybrids," *Nanoscale*, vol. 3, no. 4, pp. 1861–1873, 2011.

[19] Y. Xie and C. Yuan, "Visible-light responsive cerium ion modified titania sol and nanocrystallites for X-3B dye photodegradation," *Applied Catalysis B: Environmental*, vol. 46, no. 2, pp. 251–259, 2003.

[20] W. S. Hummers Jr. and R. E. Offeman, "Preparation of graphitic oxide," *Journal of the American Chemical Society*, vol. 80, no. 6, p. 1339, 1958.

[21] N. Huang, H. Lim, C. Chia, M. Yarmo, and M. Muhamad, "Simple room-temperature preparation of high-yield large-area graphene oxide," *International Journal of Nanomedicine*, vol. 6, pp. 3443–3448, 2011.

[22] S. Stankovich, D. A. Dikin, R. D. Piner et al., "Synthesis of graphene-based nanosheets via chemical reduction of exfoliated graphite oxide," *Carbon*, vol. 45, no. 7, pp. 1558–1565, 2007.

[23] H. Zhang, X. Zhang, D. Zhang et al., "One-step electrophoretic deposition of reduced graphene oxide and $Ni(OH)_2$ composite films for controlled syntheses supercapacitor electrodes," *The Journal of Physical Chemistry B*, vol. 117, no. 6, pp. 1616–1627, 2013.

[24] S. Ngamta, N. Boonprakob, N. Wetchakun, K. Ounnunkad, S. Phanichphant, and B. Inceesungvorn, "A facile synthesis of nanocrystalline anatase TiO_2 from $TiOSO_4$ aqueous solution," *Materials Letters*, vol. 105, pp. 76–79, 2013.

[25] Y. H. Xu, H. R. Chen, Z. X. Zeng, and B. Lei, "Investigation on mechanism of photocatalytic activity enhancement of nanometer cerium-doped titania," *Applied Surface Science*, vol. 252, no. 24, pp. 8565–8570, 2006.

[26] M. Hamadanian, A. Reisi-Vanani, and A. Majedi, "Synthesis, characterization and effect of calcination temperature on phase transformation and photocatalytic activity of Cu,S-codoped TiO_2 nanoparticles," *Applied Surface Science*, vol. 256, no. 6, pp. 1837–1844, 2010.

[27] S. Liu, H. Sun, S. Liu, and S. Wang, "Graphene facilitated visible light photodegradation of methylene blue over titanium dioxide photocatalysts," *Chemical Engineering Journal*, no. 214, pp. 298–303, 2012.

[28] C. Nethravathi and M. Rajamathi, "Chemically modified graphene sheets produced by the solvothermal reduction of colloidal dispersions of graphite oxide," *Carbon*, vol. 46, no. 14, pp. 1994–1998, 2008.

[29] F. Q. Tang, L. P. Hou, and G. S. Guo, "Preparation of TiO_2 nanometer powders," *Journal of Inorganic Materials*, vol. 16, no. 4, pp. 615–619, 2001.

[30] J. Shen, B. Yan, M. Shi, H. Ma, N. Li, and M. Ye, "One step hydrothermal synthesis of TiO_2-reduced graphene oxide sheets," *Journal of Materials Chemistry*, vol. 21, no. 10, pp. 3415–3421, 2011.

[31] X. H. Liao, J. M. Zhu, J. J. Zhu, J. Z. Xu, and H. Y. Chen, "Preparation of monodispersed nanocrystalline CeO_2 powders by microwave irradiation," *Chemical Communications*, no. 10, pp. 937–938, 2001.

[32] J. Low, J. Yu, Q. Li, and B. Cheng, "Enhanced visible-light photocatalytic activity of plasmonic Ag and graphene co-modified Bi_2WO_6 nanosheets," *Physical Chemistry Chemical Physics*, vol. 16, no. 3, pp. 1111–1120, 2014.